Electronic Supporting Information

Catalytic hydrogen production by Ni-Ru mimic of NiFe hydrogenases involves a proton-coupled electron transfer step

Sigolène Canaguier,[a] Vincent Fourmond,*[a,b] Carlo U. Perotto,[a,c] Jennifer Fize,[a] Jacques Pécaut,[d] Marc Fontecave[a,e], Martin J. Field[c] and Vincent Artero*[a]

[a] Laboratoire de Chimie et Biologie des Métaux; Université Joseph Fourier, Grenoble, France; CNRS, UMR 5249, France ; CEA, DSV/iRTSV, 17 rue des Martyrs F-38054 Grenoble Cedex 9, France. Fax: 0033 438789124; Tel: 0033 438789106; E-mail: vincent.artero@cea.fr
[b] Laboratoire de Bioénergétique et Ingénierie des Protéines, UMR 7281 CNRS-AMU 31 chemin Joseph Aiguier, 13402 Marseille, France ; E-mail: vincent.fourmond@imm.cnrs.fr
[c] DYNAMO/DYNAMOP, Institut de Biologie Structurale « Jean-Pierre Ebel », UMR CNRS/ Université Joseph Fourier/CEA 5075, 41 rue Jules Horowitz F-38027 Grenoble Cedex 1, France.
[d] Laboratoire de Reconnaissance Ionique et Chimie de Coordination; UMR-E3 Université Joseph Fourier/CEA, 17 rue des Martyrs F-38054 Grenoble Cedex 9, France.
[e] Collège de France, Grenoble, 11 place Marcellin-Berthelot 75005 Paris, France.

Experimental Section

Materials. All reactions were routinely performed under an inert atmosphere of argon using standard Schlenk techniques. Solvents were degassed and distilled under argon. Diethyl ether was distilled by refluxing over Na/benzophenone and dry dichloromethane and pentane were obtained by distillation on CaH_2. NMR solvents (Eurisotop) were deoxygenated by three freeze-pump-thaw cycles and stored over molecular sieves. Commercial dimethylformamide (DMF) for electrochemistry was degassed by bubbling nitrogen through it. [Ni(xbsms)][1] and $[Ru(C_6Me_6)Cl_2]_2$ [2] were prepared according to previously reported procedures. Commercial trifluoroacetic acid (TFA), Et_3NHCl and $AgNO_3$ were used as received. The supporting electrolyte $(n\text{-}Bu_4N)BF_4$ was prepared from $(n\text{-}Bu_4N)HSO_4$ (Aldrich) and $NaBF_4$ (Aldrich) and dried overnight at 80 °C under vacuum.

Methods and Instrumentation: NMR spectra were recorded at room temperature in 5 mm tubes on a Bruker AC 300 spectrometer equipped with a QNP probehead, operating at 300.13 MHz for ^1H and 75.5 MHz for ^{13}C. Solvent peaks are used as internal references relative to Me_4Si for ^1H and ^{13}C chemical shifts (listed in ppm). ESI mass spectra were recorded with a Finnigan LCQ thermoquest ion-trap. Elemental analyses were performed by the "Service Central d'Analyse du CNRS" (Vernaison, France). All electrochemical measurements were carried out under nitrogen at room temperature. A standard three-electrode configuration was used consisting of a glassy carbon (3 mm in diameter) or platinum (2 mm in diameter) disk as the working electrode, an auxiliary platinum wire and an Ag/AgCl/aqueous $AgCl_{sat}$ + KCl 3M (denoted as Ag/AgCl throughout this text) reference electrode closed by a Vycor frit and dipped directly into the solution.The internal reference system Fc^+/Fc was found at 0.53 V vs. Ag/AgCl in DMF. Cyclic voltammograms were recorded with a EG&G PAR 273A instrument. Solution concentrations were approximately 1 $mmol.L^{-1}$ for the catalyst and 0.1 $mol.L^{-1}$ for the supporting electrolyte $(n\text{-}Bu_4N)BF_4$. Electrodes were polished with an MD-Nap polishing pad with 1-µm monocrystalline diamond DP suspension and DP lubricant blue (Struers). Additions of TFA (50 mM solution in DMF) or Et_3NHCl (50 mM solution in DMF) were made by syringe. Cyclic voltammograms of the supporting electrolyte, Et_3NHCl and TFA in DMF have been reported elsewhere.[3-5] Bulk electrolysis experiments and coulometry were carried out on an EG&G PAR 273A instrument in DMF, using a mercury pool cathode. The platinum-grid counter electrode was placed in a separate compartment connected by a glass-frit and filled with a 0.1 $mol.L^{-1}$ solution of $(nBu_4N)BF_4$ in degassed DMF. A made-to-measure electrolysis cell with a cylindrical reservoir was used. The mercury pool surface was

therefore identical from one experiment to another. The mercury surface was measured as 1.23 cm^2 and the electrolysis cell constant was determined to be 2.34×10^{-4} s^{-1} by performing bulk electrolysis of methylviologen hexafluorophosphate.[6] The following procedure was followed: a degassed DMF solution (7 mL) containing $(nBu_4N)BF_4$ (0.1 $mol.L^{-1}$) and the acid was first electrolyzed at the desired potential until the current reached 1% of its initial value. The catalyst (1 $mmol.L^{-1}$) was then added and electrolysis was performed at the same potential with coulometric monitoring. In parallel, the volume of H_2 evolved was measured at atmospheric pressure. Hydrogen was tested for purity using a Delsi Nermag DN200 GC chromatograph equipped with a 3 m Porapack column and a thermal conductivity detector (TCD). Nitrogen under 1 bar was used as the carrier gas. The whole apparatus was thermostated at 45°C. Under these conditions, pure hydrogen has an elution time of 77 s.

Syntheses

[Ni(xbsms)Ru(C_6Me_6)](Cl) **1**(Cl)

A solution of $[Ru(C_6Me_6)Cl_2]_2$ (6,5 mg, 9,6 µmol) and [Ni(xbsms)] (7,8 mg, 19,8 µmol) in dichloromethane (5 mL) was stirred for 1 h at room temperature and then filtered through canula. The red solution is evaporated in vacuum and the red powder washed with diethylether and pentane (13 mg, 91%).
NMR ^{1}H (300 MHz, CD_3OD, 25°C): δ 7,25 (s, 4H, Ar), δ 5,34 (d, 2H, J_{AB} = 12,42 Hz, $ArCH_{eq}H_{ax}S$), 3,8 (d, 2H, J_{AB} = 12,67 Hz, $ArCH_{ax}H_{eq}S$), 2,81 (d, 2H, J_{AB} = 12,03 Hz, $(CH_3)_2C$ $CH_{eq}H_{ax}S$), 2,34 (d, 2H, J_{AB} = 12,41 Hz, $(CH_3)_2C$ $CH_{eq}H_{ax}S$), 2,07 (s, 18H, HMB), 1,68 (s, 6H, Me_{ax}), 1,40 (s, 6H, Me_{eq}). ESI-MS : m/z (%) 703 (100) $[M]^+$. Elemental analysis: calculated for **1**(Cl)·$2H_2O$ ($C_{28}H_{46}Cl_2NiRuO_2S_4$; 773,59): C 43,47; H 5,99. Experimental: C 43,75; H 6,17.

[Ni(xbsms)Ru(C_6Me_6)](NO_3) **1**(NO_3)

1(Cl) (13 mg, 18 µmol) and $AgNO_3$ (3 mg, 18 µmol) are dissolved in dichloromethane (5 mL). Immediate precipitation of AgCl is observed. After 1 h stirring in the dark, the solution is filtered through canula and evaporated in vacuum yielding a red powder (11 mg, 88%). NMR ^{1}H (300 MHz, CD_3OD, 25°C): δ 7,25 (s, 4H, Ar), δ 5,34 (d, 2H, J_{AB} = 12,42 Hz, $ArCH_{eq}H_{ax}S$), 3,8 (d, 2H, J_{AB} = 12,67 Hz, $ArCH_{ax}H_{eq}S$), 2,81 (d, 2H, J_{AB} = 12,03 Hz, $(CH_3)_2C$ $CH_{eq}H_{ax}S$), 2,34 (d, 2H, J_{AB} = 12,41 Hz, $(CH_3)_2C$ $CH_{eq}H_{ax}S$), 2,07 (s, 18H, $C_6(CH_3)_6$), 1,68 (s, 6H, Me_{ax}), 1,40 (s, 6H, Me_{eq}); ^{1}H (300 MHz, CD_2Cl_2, 25°C): δ 7,25 (m, 4H, Ar), 5,35 (d, 2H, J_{AB} = 11.90 Hz, $ArCH_{eq}H_{ax}S$), 3,60 (d, 2H, J_{AB} = 11,90 Hz, $ArCH_{ax}H_{eq}S$), 2,87 (d, 2H, J_{AB} = 12,28 Hz, $(CH_3)_2C$ $CH_{eq}H_{ax}S$), 2,17 (d, 2H, J_{AB} = 12.28 Hz, $(CH_3)_2C$ $CH_{eq}H_{ax}S$), 2,11 (s, 18H, $C_6(CH_3)_6$), 1,72 (s, 6H, Me_{ax}), 1,47 (s, 6H, Me_{eq}). ESI-MS: m/z (%) 703 (100) $[M]^+$.

Bulk electrolysis experiments

We performed a bulk electrolysis experiment on a Hg-pool cathode of a solution of **1**(Cl) (14 µmol, 7 mL) in the presence of Et_3NHCl (0.1 $mol.L^{-1}$) at –2.1 V vs Fc^+/Fc. Hydrogen evolution was monitored volumetrically at atmospheric pressure and its purity confirmed by GC analysis. During a 4 hours experiment, 45.4 C flowed through the electrode and a volume of 5.3 mL H_2 (16.8 turnovers) was evolved. This corresponds to a 97% faradaic yield. When the same experiment was performed in the presence of TFA (0.1 $mol.L^{-1}$) at –1.6 V vs Fc^+/Fc, 52.1 C flowed through the electrode and H_2 was evolved (17.1 turnovers,

89 % faradaic yield). In both cases, H_2 production was still sustained at the end of the 4 h experiment.

Overpotential determination:

We used the methodology we recently proposed[7] to determine the overpotential for H_2 evolution for both acids. For Et_3NH^+, the half-wave potential is –2.07 V vs Fc^+/Fc at 10 mmol.L^{-1}, while for TFA the half-wave potential is –1.64 V vs Fc^+/Fc at 2.4 mmol.L^{-1} (first catalytic wave). Thermodynamic predictions for the half-wave potentials for Et_3NH^+ and TFA at the same concentrations are –1.15 and –0.94 V, respectively.

Crystal Structure Analysis: Crystallographic data are summarized in Table S1. Data collection was performed at 150 K with an Oxford-diffraction diffractometer with a CCD area detector and with graphite monochromated Mo-K_α radiation (λ = 0.71073 Å). Analytical numeric absorption correction using a multifaceted crystal (Abspack[8]) was performed. Molecular structures were solved by direct methods and refined on F^2 by full-matrix least-squares techniques with the SHELXTL package,[9] with anisotropic thermal parameters. Hydrogen atoms were fixed on ideal position and refined as riding atoms. The asymmetric unit of **1**$(NO_3)\cdot CH_2Cl_2$ contains two different complexes 1^+, two nitrate anions (one in general position and two half-anions located on two-fold axis), and two CH_2Cl_2 molecules.

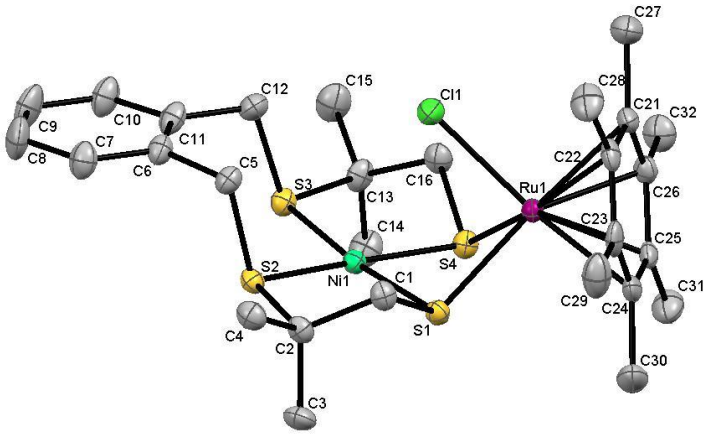

Figure S1. Fully labelled structure of the cation $\mathbf{1}^+$ in **1**$(NO_3)\cdot CH_2Cl_2$ (50% probability thermal ellipsoids).

Selected bond lengths (Å) and angles (°):

Ru(1)-C(20)	2.196(4)
Ru(1)-C(19)	2.201(4)
Ru(1)-C(18)	2.204(4)
Ru(1)-C(21)	2.209(4)
Ru(1)-C(22)	2.213(4)
Ru(1)-C(17)	2.226(4)
Ru(1)-S(4)	2.3932(11)
Ru(1)-Cl(1)	2.4062(11)

Ru(1)-S(1)	2.4106(11)
Ni(1)-S(4)	2.1678(11)
Ni(1)-S(1)	2.1783(12)
Ni(1)-S(2)	2.2130(12)
Ni(1)-S(3)	2.2132(12)
Ni(1)-S(1)-Ru(1)	90.18(4)
Ni(1)-S(4)-Ru(1)	90.90(4)

Table S1. Crystal data and structural refinement details for complex **1**$(NO_3)\cdot CH_2Cl_2$.

Compound	**1**$(NO_3)\cdot CH_2Cl_2$
Formula	C_{29} H_{44} Cl_3 N Ni O_3 Ru S4
Molecular mass	849.02
Color	dark red
Crystal size (mm)	0.70 x 0.37 x 0.12
Crystal system	monoclinic
Space group	*C 2/c*
a [Å]	46.2747(7)
b [Å]	17.1931(2)
c [Å]	18.3604(4)
α [°]	90
β [°]	107.2379(18)
γ [°]	90
V [Å]^3	13951.5(4)
Z	16
ρ_{calcd} [g.cm^{-3}]	1.617
μ [cm^{-1}]	14.74
Reflections collected	54853
Unique reflections (R_{int})	17280 (0.0386)
Observed reflections [$I>2\sigma(I)$]	17280
Refined parameters	787
R indices (all data)	R1 = 0.0550, wR2 = 0.1441
Final R indices (observed reflections)	R1 = 0.0770, wR2 = 0.1502
Goodness of fit S	1.055
$\Delta\rho$ (max/min) [e Å^{-3}]	4.491 and -1.096

$R1 = \Sigma \, | \, | F_0| - | F_c| \, | \, / \, \Sigma \, | F_0|$

$wR2 = \{\Sigma[w(F_0^2 - F_c^2)^2] / \Sigma \, [w(F_0^2)^2]\}^{1/2}$.

$w = 1 / [\sigma^2(F_0^2) + (aP)^2 + bP]$ où $P = [2F_c^2 + Max(F_0^2, 0)] / 3$ (See CIF for a and b values)

Estimation of kinetic and electrochemical parameters

Cyclic voltammograms recorded in the absence of acid

The cyclic voltammogram of **1**(Cl) recorded in DMF at 100 $mV.s^{-1}$ (Figure S2 and green trace on both panels of Figure 2) features two reduction waves at –1.48 and –1.74 V vs Fc^{+}/Fc. Their irreversible nature indicates that both reductions are followed by an irreversible chemical reaction.

Upon increasing the scan rate, the first reduction wave becomes reversible (Figure S2). This allowed us to determine both the reduction potential (E_1 = –1.47 V vs Fc^{+}/Fc) and the rate constant (k_1 = 4.7 s^{-1}) of the coupled reaction for the first wave (Figure S3). A diffusion coefficient of 1.3 $\pm 0.1 \times 10^{-6}$ $cm^2.s^{-1}$, consistent with the value we obtained for a similar complex[10], could be determined from the intensity of the first reduction wave.

We could not outrun the reaction coupled to the second reaction, even at scan rates of the order of 100 $V.s^{-1}$, which sets a lower limit on the value of its rate constant k_2 of about 2000 s^{-1}.[11] This allows an estimation of the reduction potential, assuming that this coupled reaction does not proceed faster than 10^9 s^{-1}, as: $-2.10 < E_2 < -1.80$ vs Fc^{+}/Fc.[11]

Characterization of the first catalytic wave

The first catalytic wave observed in the presence of TFA quickly saturates and levels off as acid concentration increases (Figure S5). If the rate-limiting step is the bimolecular reaction with TFA, one would expect the amplitude to grow as the square root of the acid concentration, whereas it should not depend at all on that parameter if the rate-limiting step is a first-order reaction, such as H_2 release. The relatively weak dependence of the amplitude of the catalytic wave as a function of acid concentration probably indicates that the situation is intermediate, in the sense that both a first-order reaction and the bimolecular reaction of the acid with the substrate influence the catalytic rate. Using equation 84 from ref 11, we estimate a value of ~ 30 s^{-1} for the effective first-order rate constant for this reaction.

"Total catalysis" regime (low potential catalytic wave)

To estimate a lower bound for the rate constants in the conditions of total catalysis as displayed on Figure 2 (second catalytic wave observed in the presence of TFA and sole catalytic wave observed with Et_3NH^{+}), one must keep in mind that in these conditions, the

maximum current must be lower than the value obtained in the case of plateau-shaped voltammograms. We can therefore use the greatest current obtained to set a lower limit to both the bimolecular rate constant of reaction between the complex and the acid and to the first-order rate constant of the release of H_2. Indeed, if a first-order chemical reaction step is rate-limiting, one expects the current to be given by the following formula,[11, 12]

$$I = S F n \times C_{\text{cat}} \sqrt{D k}$$

which gives, based on the maximum current shown on figure S5 right (I=400 µA, with C_{cat} = 2 mM and C_{acid} = 52.5 mM for a S=3 mm diameter electrode) a lower value for the rate-limiting first-order step of:

$k > 1300\ s^{-1}$

Similarly, if a bimolecular reaction between the complex and the acid is rate-limiting, one expects its rate constant to be larger than:

$$I = S F n \times C_{\text{cat}} \sqrt{D k_{\text{bimol}} C_{\text{acid}}}$$

$k_{bimol} > 1.10^5\ s^{-1}.L.mol^{-1}$

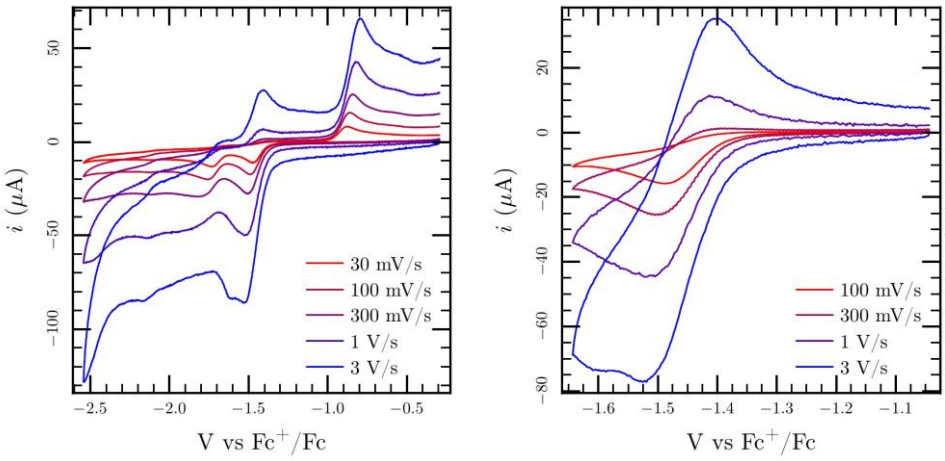

Figure S2. Cyclic voltammograms of 2 $mmol.L^{-1}$ of **1(**Cl) in DMF with 0.1 $mol.L^{-1}$ $n$$Bu_4NBF_4$ as supporting electrolyte recorded at various scan rates, in the absence of acid. Cyclic voltammograms on the right were performed with a restricted potential range to highlight the reversibility of the first wave at high scan rates.

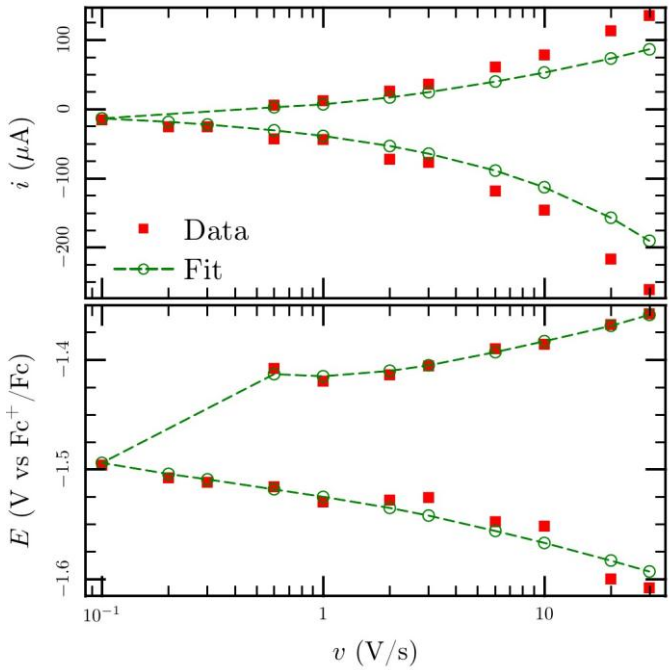

Figure S3. Top, red markers: intensity of the cathodic (negative) and anodic (positive) peaks of the first reduction wave of $\mathbf{1}^+$ as a function of scan rate. Bottom, red markers: potential of the cathodic and anodic peaks of the first reduction wave of $\mathbf{1}^+$ as a function of scan rate. Conditions as in Figure S2. Green markers and lines are curves simulated using the mechanism : $\mathbf{1}^+ + e^- \rightarrow [\mathbf{1}] \rightarrow \mathbf{[NiRu]}^+ + Cl^-$ with the following parameters: D = 1.3 $\times 10^{-6}$ $cm^2.s^{-1}$ (diffusion coefficient of all species), E^0 = –1.468 V vs Fc^+ /Fc (reduction potential), k_0 = 5.4 $\times 10^{-3}$ $cm^{-1}.s^{-1}$ (interfacial electron transfer rate constant) and k = 4.7 s^{-1} (the follow-up rate constant). Discrepancies between the fit and the data at high scan rates arise from the electrode charging (capacitive) current.

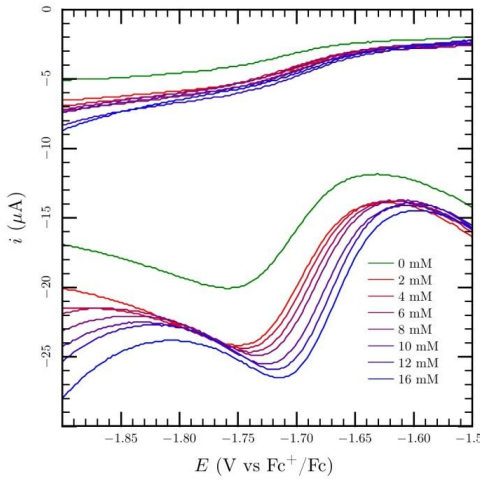

Figure S4. Zoom (from Figure 2) on the second reduction wave of **1**(Cl) in the presence of increasing amounts of Et_3NH^+. Conditions identical to those of Figure 2.

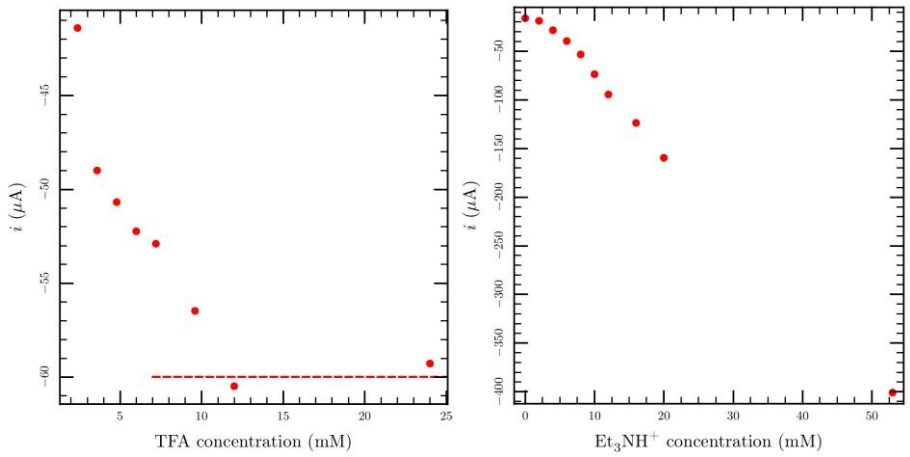

Figure S5. Left: amplitude of the first catalytic reduction wave in presence of TFA as a function of TFA concentration and right: amplitude of the sole catalytic reduction wave in the presence of Et_3NH^+. All conditions are identical to that of Figure 2.

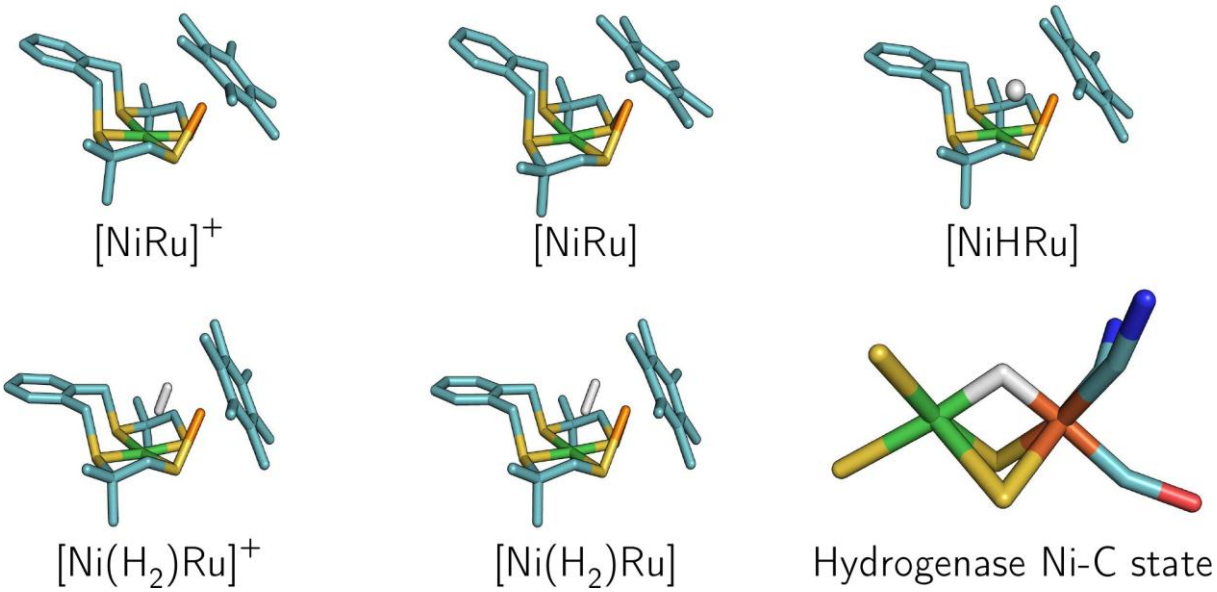

Figure S6. DFT-optimized structures of the intermediates involved in the catalytic cycle and structure of the Ni-C state of NiFe-hydrogenase.

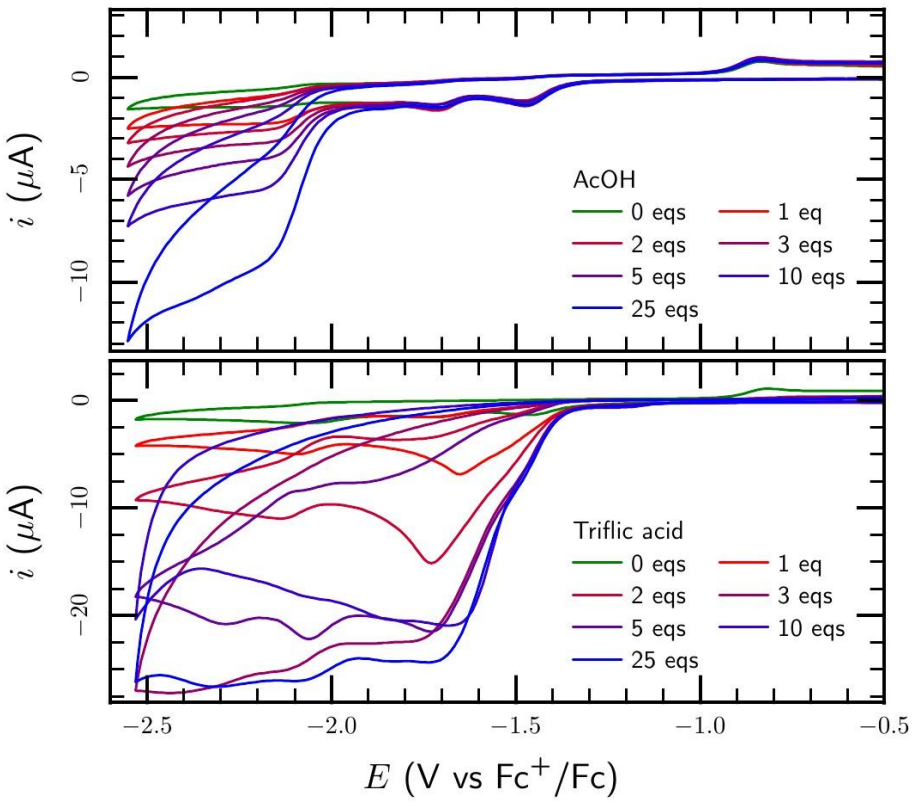

Figure S7. Cyclic voltammograms of **1**(Cl) (1 mmol.L^{-1}) in DMF with 0.1 mol.L^{-1} *n*Bu_4NBF_4 as supporting electrolyte in the presence of acetic acid (AcOH, top) and triflic acid (bottom).

DFT calculations

DFT calculations were performed with the Jaguar quantum chemistry program (version 5.2) using the crystallographic structure of [Ni(xbsms)RuCl(C_6Me_6)](NO_3).[13] Calculations were carried out with two different functionals, B3LYP and BP86, and the LACV3P**++ basis set, which is of triple-zeta quality and has polarization and diffuse functions. For each modelled species in the catalytic cycle, geometry optimizations were carried out first in the gas-phase followed by optimization with an implicit solvent model (Poisson-Boltzmann solver) corresponding to DMF.

Table S2. Comparison of the X-ray and gas-phase DFT-optimized structures of **1**$^+$. The two numbers for the X-ray structure correspond to the two different molecules in the unit cell.

Bond (Å)/angle (°)	X-ray structure determination	DFT/B3LYP	DFT/BP86
Ni-Ru	3.249/3.269	3.297	3.275
Ru-Cl	2.404/2.398	2.462	2.446

Ni-Cl	3.120/3.139	3.114	3.019
Ru-S_1	2.407/2.386	2.460	2.436
Ru-S_4	2.380/2.417	2.459	2.442
Ni-S_1	2.173/2.173	2.236	2.224
Ni-S_4	2.173/2.172	2.235	2.225
S_1-Ru-S_4	71.9/71.4	73.0	72.5
S_1-Ni-S_4	80.6/80.3	81.8	80.8
Ni-S_1-Ru	90.2/91.5	89.0	89.2
Ni-S_4-Ru	91.0/90.7	89.1	89.0
Hinge Ni-2S-Ru	129.1/129.5	127.9	126.7
Hinge 2S-Ni-2S	176.1/175.8	177.6	179.5

Table S3. Structural data for the intermediate species in the H_2-evolving catalytic cycle of **1**$^+$ (B3LYP in DMF)

Bond (Å)/angle (°)	**[NiRu]**$^+$ (Initial and final steps)	**[NiRu]**	**[NiHRu]**	**[NiRu(H_2)]**$^+$	**[NiRu(H_2)]**
Ni-Ru	2.850	3.131	3.042	3.219	3.249
Ru-H_1			1.613	1.739	1.965
Ru-H_2				1.762	1.982
Ni-H_1			2.343	3.113	3.270
Ni-H_2				2.260	2.500
Ni-H_1-Ru			98.8	77.4	71.9
Ni-H_2-Ru				105.6	92.2
Hinge Ni-2S-Ru	108.6	120.9	115.9	123.2	127.1
Hinge 2S-Ni-2S	172.3	166.8	170.3	165.9	167.7

Table S4. Mulliken spin densities for the intermediate species in the H_2-evolving catalytic cycle of $\mathbf{1}^+$ (B3LYP in DMF)

Atom	**[NiRu]$^+$** (Initial and final steps)	**[NiRu]**	**[NiHRu]**	**[NiRu(H_2)]$^+$**	**[NiRu(H_2)]**
Ru	-0.194	0.891	-0.009	-0.011	-0.839
Ni	0.965	-0.803	0.833	0.825	0.833
H_1			0.002	-0.001	-0.045
H_2				-0.001	-0.014
S_1	0.078	-0.046	0.052	0.063	0.047
S_2	0.082	-0.051	0.051	0.048	0.051
S_3	0.054	-0.042	0.037	0.044	0.035
S_4	0.054	-0.042	0.038	0.035	0.035

Table S5. Atomic (ESP) charges for the intermediate species in the H_2-evolving catalytic cycle of $\mathbf{1}^+$ (B3LYP in DMF except for X-ray which was optimized in the gas phase)

Atom	$\mathbf{1}^+$	$\mathbf{[NiRu]^+}$	**[NiRu]**	**[NiHRu]**	$\mathbf{[NiRu(H_2)]^+}$	**[NiRu(H$_2$)]**
Ru	0.524	0.315	0.423	0.704	0.552	0.522
Ni	0.422	0.490	0.347	0.252	0.274	0.258
Cl	-0.495					
H_1				-0.245	0.224	-0.183
H_2					0.211	0.260
S_1	-0.400	-0.453	-0.639	-0.561	-0.538	-0.574
S_2	-0.402	-0.477	-0.613	-0.558	-0.495	-0.533
S_3	-0.236	-0.337	-0.368	-0.244	-0.317	-0.274
S_4	-0.201	-0.320	-0.338	-0.234	-0.231	-0.275
Total 4S	-1.239	-1.587	-1.808	-1.597	-1.581	-1.656

Table S6. Structural data for the intermediate species in the H_2-evolving catalytic cycle of $\mathbf{1}^+$ (BP86 in DMF)

Bond (Å)/angle (°)	**[NiRu]$^+$** (Initial and final steps)	**[NiRu]**	**[NiHRu]**	**[NiRu(H_2)]$^+$**	**[NiRu(H_2)]**
Ni-Ru	2.820	2.893	2.881	3.064	2.957
Ru-H_1			1.660	1.702	1.649
Ru-H_2				1.783	1.725
Ni-H_1			1.948	2.866	2.883
Ni-H_2				1.926	1.845
Ni-H_1-Ru			105.7	79.8	76.1
Ni-H_2-Ru				111.3	111.8
Hinge Ni-2S-Ru	107.9	109.6	106.4	113.7	107.1
Hinge 2S-Ni-2S	175.1	170.1	175.8	171.3	176.1

Table S7. Mulliken spin densities for the intermediate species in the H_2-evolving catalytic cycle of $\mathbf{1}^+$ (BP86 in DMF)

Atom	**[NiRu]$^+$** (Initial and final steps)	**[NiRu]**	**[NiHRu]**	**[NiRu(H_2)]$^+$**	**[NiRu(H_2)]**
Ru	-0.094	0.716	-0.003	-0.009	-0.496
Ni	0.725	-0.549	0.670	0.653	0.583
Cl					
H_1			0.000	-0.001	0.009
H_2				-0.009	-0.009
S_1	0.132	-0.073	0.096	0.104	0.020
S_2	0.092	-0.078	0.096	0.102	0.056
S_3	0.080	-0.074	0.067	0.074	0.056
S_4	0.087	-0.074	0.067	0.075	0.105

Table S8. Atomic (ESP) charges for the intermediate species in the H_2-evolving catalytic cycle of $\mathbf{1}^+$ (BP86 in DMF except for X-ray which was optimized in the gas phase)

Atom	$\mathbf{1}^+$	$\mathbf{[NiRu]^+}$	**[NiRu]**	**[NiHRu]**	$\mathbf{[NiRu(H_2)]^+}$	**[NiRu(H_2)]**
Ru	0.459	0.344	0.463	0.547	0.284	0.297
Ni	0.312	0.433	0.317	0.207	0.277	0.262
Cl	-0.406					
H_1				-0.231	0.042	0.021
H_2					0.005	-0.112
S_1	-0.327	-0.426	-0.558	-0.470	-0.385	-0.452
S_2	-0.339	-0.423	-0.594	-0.471	-0.380	-0.483
S_3	-0.211	-0.309	-0.362	-0.224	-0.222	-0.236
S_4	-0.183	-0.297	-0.317	-0.229	-0.238	-0.222
Total 4S	-1.061	-1.456	-1.832	-1.394	-1.225	-1.392

References

1. J. A. W. Verhagen, D. D. Ellis, M. Lutz, A. L. Spek and E. Bouwman, *Dalton Trans.*, 2002, 1275-1280.
2. M. A. Bennett, T. N. Huang, T. W. Matheson and A. K. Smith, *Inorg. Synth.*, 1982, **21**, 74-78.
3. S. Canaguier, M. Field, Y. Oudart, J. Pecaut, M. Fontecave and V. Artero, *Chem. Commun.*, 2010, **46**, 5876-5878.
4. C. Baffert, V. Artero and M. Fontecave, *Inorg. Chem.*, 2007, **46**, 1817-1824.
5. M. Razavet, V. Artero and M. Fontecave, *Inorg. Chem.*, 2005, **44**, 4786-4795.
6. Y. Oudart, V. Artero, J. Pécaut, C. Lebrun and M. Fontecave, *Eur. J. Inorg. Chem.*, 2007, 2613-2626.
7. V. Fourmond, P. A. Jacques, M. Fontecave and V. Artero, *Inorg. Chem.*, 2010, **49**, 10338-10347.
8. *CrysAlis PRO. Agilent Technologies, Yarnton, England.*
9. G. M. Sheldrick, *SHELXTL Version 6.1 (1997); Bruker AXS Inc., Madison, Wisconsin, USA.*
10. V. Fourmond, S. Canaguier, B. Golly, M. J. Field, M. Fontecave and V. Artero, *Energy Environ. Sci.*, 2011, **4**, 2417-2427.
11. R. S. Nicholson and I. Shain, *Anal. Chem.*, 1964, **36**, 706-723.
12. J. M. Savéant and E. Vianello, *Langmuir, I. (ed.) Advances in polarography Ed. Pergamon Press*, 1960, **1**, 367-374.

13. Jaguar 5.2, Schrödinger L.L.C., Portland and OR, 2003.